

Estimating annual apparent thermal diffusivity in permafrost using temperature time series on the Qinghai-Tibet Plateau, China

Xie Changwei¹ William A. Gough² Zhao Lin¹ Wu Tonghua¹

¹ Cryosphere Research Station on the Qinghai-Tibet Plateau, State Key Laboratory of Cryospheric Sciences, Cold & Arid Regions Environmental and Engineering Research Institute, Chinese Academy of Sciences, Lanzhou, China

² Department of Physical & Environmental Sciences, University of Toronto-Scarborough, Toronto, M1C 1A4, Canada



*Challenges from North to South
Des défis du Nord au Sud*

ABSTRACT

Soil temperature data used in this study were obtained from 17 monitoring boreholes during the period from 2006 to 2010 on the Qinghai-Tibet plateau. Measurements show that the permafrost temperature is higher than -1.0°C at eleven sites and at eight sites it is higher than -0.5°C . We calculated the annual apparent thermal diffusivity (AATD) in permafrost at different horizons. Results indicate that the latent heat effects have important implications for the permafrost thermal regime. In warm permafrost regions, the latent heat effects buffered heat exchange and resulted in shallow depths of zero annual amplitude (DZAA) of ground temperature and AATD. At the same sites, thermal diffusivity is usually lower at the bottom of the active layer since ice-water conversion consumes most of the heat exchange at this horizon. The thermal diffusivity is usually larger in the deep permafrost especially when the permafrost temperature is low. For the 17 monitoring boreholes, there is a causal relationship between the small AATD and the high permafrost temperature. The temperature-dependent adjustments of the thermal diffusivity have important implications for the warming trend of permafrost. The permafrost temperature gradient is greater in cold permafrost with large AATD than it is in warm permafrost with small AATD.

RÉSUMÉ

Les mesures de la température du sol utilisées dans cette étude ont été obtenues à l'aide de 17 forages en observation pendant une période de 2006 à 2010 sur le plateau Qinghai-Tibet. Les données montrent que la température du pergélisol est plus élevée que -1.0°C à onze sites et plus élevée que -0.5°C à huit sites. Nous avons calculé la diffusivité thermique apparente annuelle (AATD) dans le pergélisol à différents horizons. Les résultats indiquent que les effets de la chaleur latente ont des implications importantes pour le régime thermique du pergélisol. Dans les régions chaudes du pergélisol, les effets de la chaleur latente ont tamponné l'échange de chaleur et ont résulté en des profondeurs superficielles d'une amplitude annuelle de zéro (DZAA) de la température du sol et de l'AATD. Aux mêmes sites la diffusivité thermique est habituellement plus basse au bas de la couche active, étant donné que la conversion glace-eau consomme la plus grande partie de l'échange thermique à cet horizon. La diffusivité thermique est habituellement plus large dans les profondeurs du pergélisol, particulièrement quand sa température est basse. Pour les 17 forages en observation, il y a une relation de cause entre une petite AATD et une température du pergélisol élevée. Les ajustements de la diffusivité thermique qui dépendent de la température ont d'importantes implications dans la tendance d'évolution du pergélisol. Le gradient de température du pergélisol est plus grand dans un pergélisol froid avec une AATD large que dans un pergélisol chaud avec une petite AATD.

1 INTRODUCTION

The Qinghai-Tibet Plateau (QTP) has the largest expanse, about $1.3 \times 10^6 \text{ km}^2$, of elevational permafrost on earth. Warm permafrost, which is defined as permafrost temperature at or higher than -1.0°C (Wu and Zhang, 2008), is widely distributed in the QTP while permafrost with temperature below -2.0°C is restricted to some high mountain areas. Under recent climate warming, the degradation of permafrost and the resulting impacts in the past several decades have caused widespread concern. Research has shown that there is a large variation in the magnitude of permafrost temperature change within the QTP. During the 1996-2006 period, the rate of permafrost temperature increase was usually less than $0.3^{\circ}\text{C}/10\text{y}$ at sites with long-term mean permafrost temperature at or above -1.0°C , whereas at sites with long-term mean permafrost temperature lower than -2.0°C , the rate of permafrost temperature increase was greater than

$0.5^{\circ}\text{C}/10\text{y}$ (Wu and Zhang, 2008). In contrast, the magnitude of active-layer thickness (ALT) increase is greater in warm permafrost regions than in cold permafrost regions. The average rate of the ALT increase is about 5.0 cm/y in cold permafrost regions, whereas in warm permafrost areas, the mean rate of increase is as much as 11.2 cm/y from 1995 to 2007 (Wu and Zhang, 2010). These observations suggest there are connections between the permafrost thermal regime and the change trend of permafrost. By means of diagnostic analysis of permafrost thermal regime under different temperature conditions, we may fully estimate the overall change trend of permafrost on the QTP.

Accurate interpretation of the difference in the change trend of permafrost with different thermal regime requires an understanding of the temperature-dependent adjustments of soil thermal properties, i.e., thermal conductivity (λ), thermal diffusivity (κ), and volumetric

heat capacity (C_g). Thermal diffusivity is a crucial parameter for analyzing the ground thermal regime and is the only parameter that can be calculated by ground temperature data series. For example, using the ratio amplitude method, Hinkel (1997) calculated the diffusivity by relating the average temperature change rates at different horizons in the active layer and near-surface permafrost at two sites in northern Alaska. Based on hourly measurements over the Naqu area on the QTP, Gao et al. (2002) calculated the apparent soil thermal diffusivity in the active layer by the analytic solution to the soil thermal conduction equation with the thermal convection term explicitly represented. Due to limitations of the measurement data and the calculation methods, the soil thermal diffusivity is always estimated only in shallow horizons or in active layers in permafrost regions. During last two decades, temperature measurements in boreholes have been continuously recorded in permafrost regions by automated instruments. These data can be easily used to derive vertical profiles and time series data and can be used to estimate apparent thermal diffusivity in deep permafrost. This work will use continuous data obtained from 17 monitoring sites on the QTP to calculate the annual apparent thermal diffusivity at different depths in permafrost on the QTP. The aim of this paper is to analyze the relationship between the permafrost thermal regime and the change trend of permafrost temperature.

2 METHOD

Time dependent heat flow is usually described by the conduction heat transfer equation:

$$\frac{\partial T}{\partial t} = \kappa \frac{\partial^2 T}{\partial z^2} \quad (1)$$

where κ is the soil thermal diffusivity (m^2/s) and is defined as the ratio of the thermal conductivity (λ) and the volumetric heat capacity (C); T is the soil temperature, t is the time and z is the depth. Various methods have been developed to estimate the thermal diffusivity in soils from temperature time series and most of these algorithms are based on solutions of the one-dimensional conduction heat transfer equation (i.e., Amplitude, Phase, Arctangent, Logarithm, and Harmonic or HM algorithms). All these algorithms have limitations and a review of these methods can be found in Horton (1983) and Gao et al. (2009). In order to incorporate the effects of latent heat when substantial phase change is involved, some researchers have tried to use another kind of approach to calculate "apparent" thermal diffusivity by evaluating the $\partial T / \partial t$ and $\partial^2 T / \partial z^2$ at a particular time and depth. For example, using finite difference methods, Zhang et al. (1999) have taken into account the accuracy of the temperature measurements, duration and amplitude of the temperature changes to evaluate the apparent thermal diffusivity in active layer and permafrost. This kind of method requires highly accurate measurements ($\pm 0.01^\circ C$) and the amplitude of the temperature time series. However, at deep horizons in permafrost, especially under the depth of zero annual amplitude (DZAA) of ground

temperature, $\partial T / \partial t$ and $\partial^2 T / \partial z^2$ are very small and cannot be detected by the instruments at a particular time. Hence this kind of approach also has limitations. In this study, we use the Amplitude and Phase algorithm to roughly estimate the annual apparent thermal diffusivity (AATD). The aim of this work is to compare the difference in the thermal diffusivities at different depths in different permafrost regions by a unified method. A brief introduction of the methods follows.

In permafrost, the general features of the thermal regime in the layer of annual variations, such as the exponential attenuation of seasonal wave with depth and the lag in phase, can be analyzed using the heat conduction equation with a sinusoidal surface temperature variation (Williams and Smith 1989). The temperature at any depth, z , is given by Ingersoll et al

$$(1954): \quad T(z, t) = \bar{T}_z + A_s e^{-z(\omega/2\kappa)^{1/2}} \sin\left[\omega \cdot t - \left(\frac{\omega}{2\kappa}\right)^{1/2} \cdot z\right] \quad (2)$$

where $\omega = 2\pi / P$, P is the period of the wave (one year), and A_s is the amplitude of the surface temperature wave. Time t is counted from the date in spring when the surface temperature wave passes through its mean annual value. The expression:

$$A_z = A_s e^{-z(\omega/2\kappa)^{1/2}} = A_s e^{-z(\pi/\kappa P)^{1/2}} \quad (3)$$

represents the amplitude of the temperature wave at depth z , and the term

$$t_z = z \left(\frac{1}{2\kappa\omega} \right)^{1/2} = \frac{z}{2} \left(\frac{P}{\pi\kappa} \right)^{1/2} \quad (4)$$

is the lag of the wave with depth.

If we take the ratio of the amplitude at two depths, z_1 and z_2 , we can get the Amplitude algorithm for calculating the thermal diffusivity:

$$\kappa = \frac{\pi}{P} \left(\frac{z_2 - z_1}{\ln A_1 / A_2} \right)^2 \quad (5)$$

If we compare the lag at two depths, we can get the Phase algorithm as follows:

$$\kappa = \frac{P}{4\pi} \left(\frac{z_2 - z_1}{t_2 - t_1} \right)^2 \quad (6)$$

From the forms of formulae 5 and 6, it follows that when $\ln(A_1/A_2)$ and $t_2 - t_1$ are close to zero, a slight change of these two values will cause dramatic changes in the value of κ . When the amplitude at depth z_1 is close to the amplitude at depths z_2 , the calculation errors of the Amplitude algorithm will be large. The Amplitude algorithm should be suitable only for the case that the amplitudes at two depths have clear differences. Similarly, the Phase algorithm should only be used when there is a clear difference in the lag time at the two depths.

The temperature at the DZAA is usually considered as the mean annual temperature of permafrost. The operational definition for the DZAA is the depth where the annual wave is delayed by exactly one year from that at the surface (Williams and Smith 1989). From formula 4, the DZAA can be calculated as follows:

$$DZAA = 2(\pi\kappa P)^{1/2} \quad (7)$$

Hence, we can also estimate the average AATD for horizons above the DZAA at those sites:

$$\kappa = \frac{(DZAA)^2}{4\pi P} \quad (8)$$

3 STUDY AREA AND DATA

During the past several decades, permafrost has been increasingly studied on the QTP (Figure 1). Most of the studies are concentrated along the Qinghai-Xizang Highway (QXHW) and the Qing-Kang Highway due to the region's isolation and harsh environmental conditions in the hinterland of the QTP (Cheng and Wu, 2007; Jin et al., 2008, Wu et al., 2010; Zhao et al., 2010; Xie et al., 2012). Thousands of boreholes were drilled into the permafrost for the engineering design and construction of the Qinghai-Xizang Railway and for scientific research programs. Since the 1980s, an integrated permafrost monitoring network including more than 20 boreholes with depths from 20 to 127 m has been set up along the QXHW (Cheng and Wu, 2007; Zhao et al., 2010; Xie et al., 2012). All the boreholes are located at least 2 to 5 kilometers away from the highway in order to avoid the direct influence of the QXHW. Thermistor sensors were installed on cables and were permanently installed into these boreholes, which were cased using 5 cm diameter steel pipes (Zhao et al., 2010). Generally, the thermistor sensors were deployed at 1 m intervals near the surface ($\leq 6-8$ m) and 2-3 m intervals at greater depths. These thermistor sensors, which were made at the Chinese State Key Laboratory of Frozen Soil Engineering at Lanzhou, are highly sensitive (± 0.01 °C) in laboratory tests (Cheng and Wu, 2007). Initially, soil temperatures at different levels were measured three times per month by hand and then averaged over a year. Automated data-loggers have been subsequently installed to record temperatures and water content at various horizons in the active layer since 1998, and have been commonly used to record ground temperatures at different depths in permafrost since 2005. At the present time, all sites are equipped with Campbell Scientific, Inc. data-loggers (Model: CR10X, CR1000 or CR3000) to record the measurements (Zhao et al., 2010).

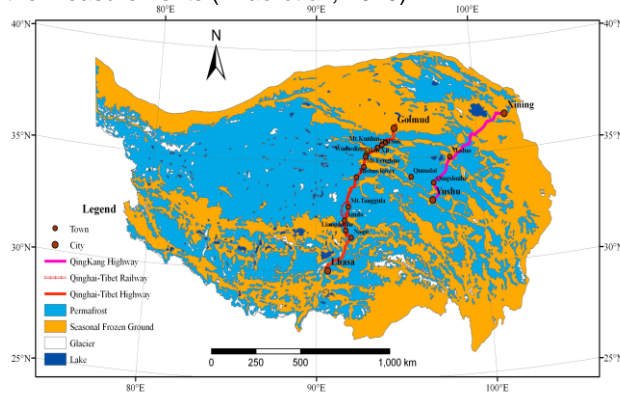


Figure 1 Map of permafrost distribution on the Qinghai-Tibet Plateau (adapted from Cheng and Wu, 2007)

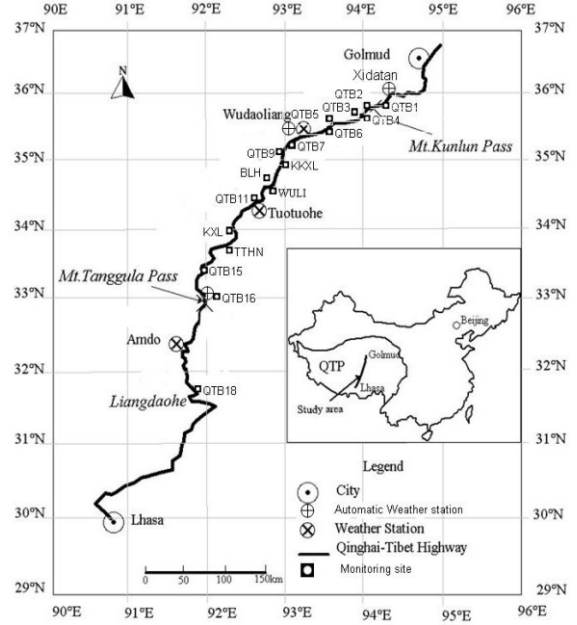


Figure 2 The locations of 17 monitoring sites along the QXHW on the QTP

Soil temperature data used in this study were obtained from 17 monitoring boreholes along the QXHW during the 2006 to 2010 period (Figure 2). Permafrost temperatures in all of these boreholes are automatically recorded 12 times per day at 2-hour intervals during the study period. Tables 1 and 2 summarize geographical locations, soil type, vegetation cover, permafrost conditions and monitoring period at each site. The soil types are observed near the surface and varied from fine materials as clay to silt/sand/gravel, consistent with Wu and Zhang (2008; 2010). At some sites, soil temperature and water content were both monitored at many horizons in the active layer, such as XDT, QTB02, QTB09, QTB16 and QTB18.

In this study, meteorological data are collected from three automated weather stations (AWS) that are located in Xidatan, Wudaoliang and Tanggula (Figure 2). Air temperature and precipitation have been continuously observed at these three meteorological stations during the study period. Long-term meteorological data are provided by three Chinese National Meteorological Stations (CNMS), which are located in Wudaoliang, Tuotuohe and Amdo. In addition, air temperature was also observed at 0.5 m above the surface at these monitoring sites (boreholes) during the study period. Thus, for each of the permafrost monitoring sites in this study, the air temperature can be obtained either locally or from nearby weather stations.

Table 1 Geographical data and information of 17 monitoring sites on the QTP (List at the end of the paper)

Table 2 Climatic and environmental parameters at 17 monitoring sites on the QTP (List at the end of the paper)

4 RESULTS AND DISCUSSION

4.1 Permafrost thermal regime and the AATD

On the QTP, warm permafrost is widely distributed in Xidatan basin, Chumaer River basin, Tuotuohe River basin and in the south of Tanggula Mountains. Permafrost with temperature below -2.0°C was only found at three sites, QTB2, QTB9 and KKXL. QTB2 is located at the south-facing slope of Kunlun Mountains and both QTB9 and KKXL are located in the Hoh Xil Mountains. Figure 3 shows the permafrost temperature (the mean annual ground temperature at the depth of zero annual amplitude (DZAA, Qiu *et al.* 1994) at all of the 17 monitoring sites along the QXHW. Eleven permafrost sites are classified as warm permafrost, which is defined as permafrost temperature at or higher than -1.0°C (Wu and Zhang, 2008), and eight of them are warmer than -0.5°C . Since the thermal diffusivity is equal to the ratio of the thermal conductivity (λ) and the volumetric heat capacity (C), with the increasing temperature, the effect of decreasing conductivity and increasing apparent heat capacity results in a decreasing thermal diffusivity. Within the range 0 to -3.0°C , the thermal diffusivity of permafrost is highly temperature dependent and is dominated by the heat capacity term (Williams and Smith, 1989). On the QTP, AATD is highly influenced by permafrost thermal regime since permafrost temperature in most regions is just within the range 0 to -3.0°C .

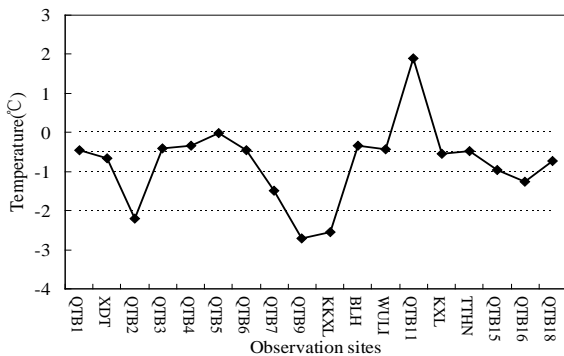


Figure 3 Permafrost temperatures (the mean annual ground temperature at the DZAA in 2010) at 17 monitoring sites along the QXHW

Figure 4 shows the calculated AATD at different horizons above DZAA for all the 17 observation sites. It can be seen that the AATD changes dramatically at different horizons. Generally, AATD is relatively small in the active layer, especially at the horizons close to the bottom of the active layer. In the active layer, the main energy exchange is used to thaw and freeze the soil, thus the soil apparent heat capacity is large and AATD becomes small. At the bottom of the active layer, soil usually contains more moisture, which consumes more energy exchange and results in small AATD. In deep permafrost, AATD is generally smaller than $1.0 \times 10^{-6} \text{ m}^2/\text{s}$ at most horizons at those sites with high permafrost temperatures. For example, QTB6 is located on the southern Qingshuihe river terraces where the DZAA is 3.9 m and permafrost temperature is -0.35°C . AATD at all the horizons is less than $0.2 \times 10^{-6} \text{ m}^2/\text{s}$ and the average AATD is only $0.098 \times 10^{-6} \text{ m}^2/\text{s}$ above the DZAA. At these

sites, ice-rich weathered marl developed near the permafrost table and the thermal regime of permafrost is controlled by latent heat effects, which results in small AATD at these sites.

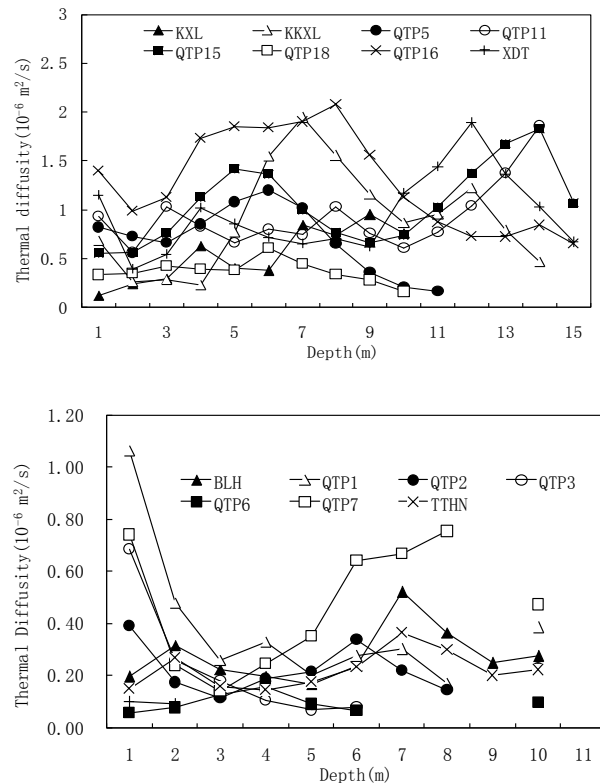


Figure 4 Calculated AATD at different horizons above DZAA for all the 17 observation sites

At sites with permafrost temperature lower than -1.0°C , AATD at some horizons is larger than $1.5 \times 10^{-6} \text{ m}^2/\text{s}$ and the average AATD is larger than that for warm permafrost sites. These large AATDs are due to the frozen state as well as the structure of the soil. Under the frozen state, the latent heat effects are weak and the apparent volumetric heat capacity is small, which resulted in large AATDs. At the same time, when the soil texture is loose, AATDs are large since the soil pore space is filled by air. Its thermal diffusivity is larger than ice and most minerals. At QTB16, which is located on an ancient glacial till at the north-facing slope of Tanggula Mountains and permafrost temperature is -1.3°C , the AATD is larger than $1.50 \times 10^{-6} \text{ m}^2/\text{s}$ between 4.0 m to 10.0 m depth. Glacial till is that part of glacial drift which was deposited directly by the glacier. Its content always varies from clays to mixtures of clay, sand, gravel and boulders, which is conducive for downward heat transmission.

Using formula 7, the DZAA at all the 17 observation sites can be determined using the continuous temperature data series and the average AATD can be determined by formula 8. Figure 5 shows the scatterplot relationship between permafrost temperatures and the average AATD

at every site. It can be seen that permafrost thermal regime has important implications on the patterns of the AATD. There is a positive relationship between small average AATD and high permafrost temperature. At all of the sites with permafrost temperature higher than -0.5°C , the average values for AATD above the DZAA are smaller than $0.22 \times 10^{-6} \text{ m}^2/\text{s}$, while for the sites with permafrost temperature lower than -1.0°C , the values are larger than $0.56 \times 10^{-6} \text{ m}^2/\text{s}$. At those sites with high permafrost temperature, the latent heat effects buffered the heat exchange in permafrost and results in large apparent volumetric heat capacity, thus reduced the values of DZAA and AATD.

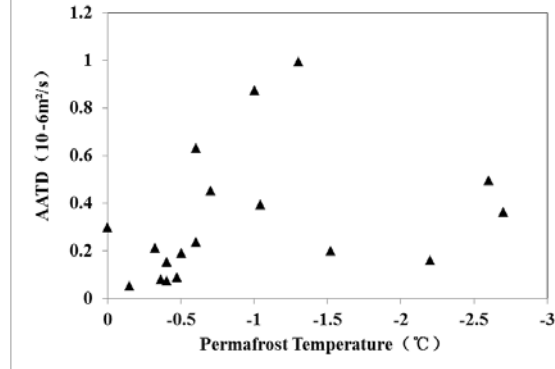


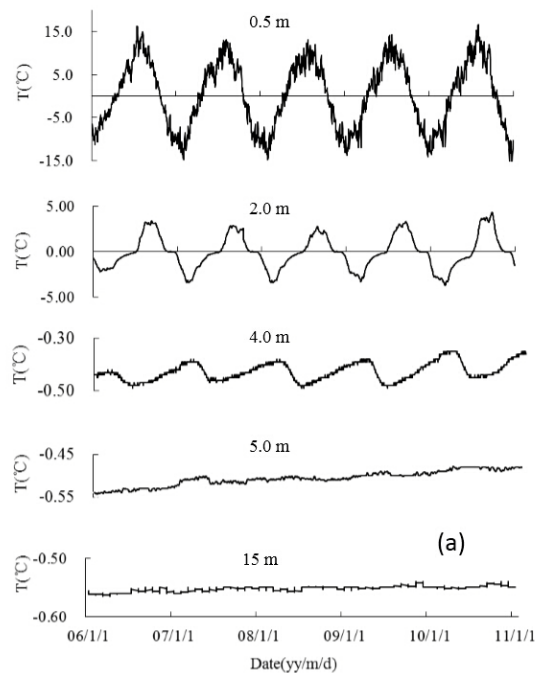
Figure 5 Scatterplot between permafrost temperature and the average AATD at 17 monitoring sites

4.2 Thermal diffusivity and permafrost warming

In permafrost regions, fluctuations of air temperature were attenuated with depth in the permafrost. The attenuation rate is different at different sites. The temperature wave was attenuated rapidly at those sites with small DZAA while it is attenuated slowly at the sites with large DZAA. For example, at QTP6 (Figure 6a), the ground temperatures at 0.5 m and 2.0 m depth have the same change trend as that of air temperature. However, at 5.0 m (DZAA at this site is 3.1m), the yearly fluctuations of the temperature were significantly reduced and there were no obvious peak and valley values in the temperature record. At QTP15 (Figure 6b), permafrost temperature is relative low (-1.03°C) and the DZAA is comparatively large (14.2m). The yearly fluctuations can be easily detected at 15.0 m and the lag time increases quickly in the deep horizons. The change trend of permafrost temperature in deeper horizons is not consistent with the current climate change but reflects the comprehensive climate change over a past period. In many studies, the warming trend of permafrost was detected at a specific depth, such as that discussed by Wu and Zhang (2008) and Zhao et al. (2010). In fact, the warming trend at a specific depth cannot reflect the real warming trend in the permafrost. The warming trend at the DZAA should be more representative. In this study, we discuss warming trend at the DZAA.

During the observation period, all of the sites show a continuous warming trend and the average warming rate is $0.017^{\circ}\text{C}/\text{y}$. The maximum warming rate is $0.031^{\circ}\text{C}/\text{y}$, which was found at KKXL where permafrost temperature is -2.6°C . The minimum rate is only $0.004^{\circ}\text{C}/\text{y}$, which was

found at QTP4, where permafrost temperature is -0.4°C . The spatial distribution of warming rate along the QXHW is generally controlled by permafrost temperature while the surface condition and regional climate have important effects. In Xidatan, the warming rate at QTB1 is $0.013^{\circ}\text{C}/\text{y}$, which is smaller than that at XDT ($0.021^{\circ}\text{C}/\text{y}$). The difference at the two sites is closely linked with the regional environment and permafrost temperature. Along the QXHW (Figure 7), warming rate is relatively high at Kunlun Mountain site (QTB2) where permafrost temperature is relatively low. In the Chumaer River basin warming rates at most sites are relatively low since permafrost temperatures at these sites are high and the DZAA is typically small. High warming rates are found at the two sites in HohXil Mountains, where permafrost is relatively cold. The warming trend is very weak at Tanggula Mountains site (QTB16) although the permafrost temperature is low and the DZAA is very high. It is interesting that the warming trend at this site is weak. Wu and Zhang (2008) reported that soil temperatures within the active layer and upper permafrost show a slight decreasing trend at TG1 observation site in this region over a period from 1999 through 2006. The TG1 site is located at approximately 50 km south to QTP16 site. Wu and Zhang (2008) inferred that the increased precipitation in this region may lead to the slight decreasing trend of the permafrost temperature. Further monitoring at this site is needed to better explain the cooling trend. At the south of Tanggula Mountains, the warming rate is 0.023 at QTP18, which is greater than the average value. In addition, the warming rate ($0.024^{\circ}\text{C}/\text{y}$) of permafrost at QTB11 site, which is the only observation site that locates in non-permafrost region, is larger than the average warming rate ($0.017^{\circ}\text{C}/\text{y}$). When the permafrost is completely degraded, there are no latent heat effects and the soil will warming quickly under same climate warming.



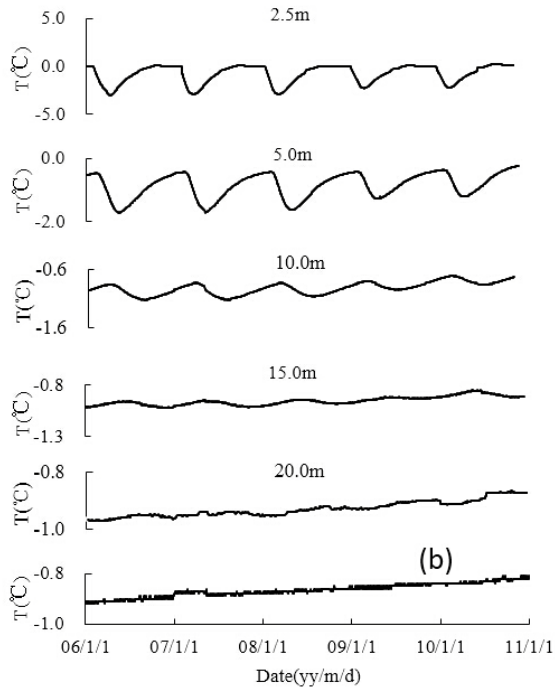


Figure 6 Variations of daily ground temperature at different depths at QTP 6(Above) and QTP15 (Below) during 2006 to 2010.

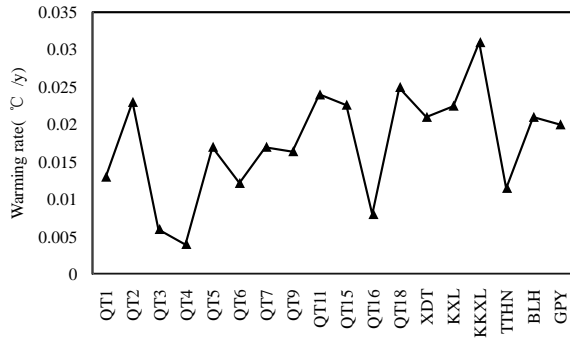


Figure 7. Warming rates of permafrost temperature along the Qinghai-Xizang Highway

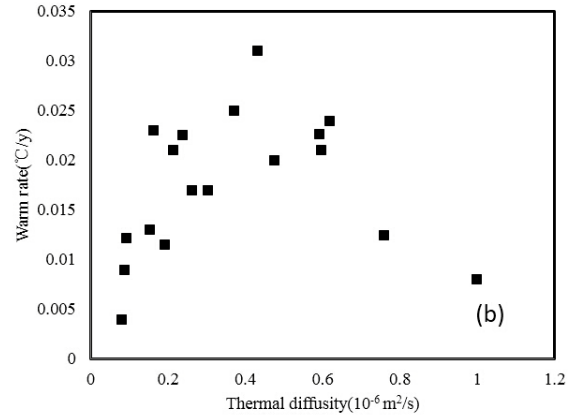
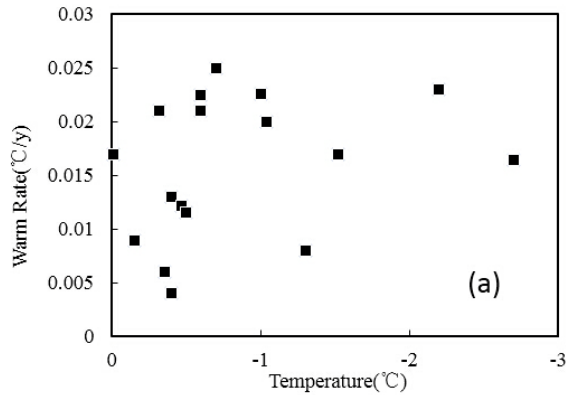


Figure 8 Scatter relations between permafrost warming rate and permafrost temperature (a) and the AATD (b)

Close relationships are found between the warming trend of permafrost and permafrost temperature. From Figure 8a, it can be seen that there is a roughly negative relationship between the warming rates and permafrost temperatures at those observation sites (except the QTP11). The average warming rate for permafrost with low temperatures ($<-1.5\text{ }^{\circ}\text{C}$) is $0.020\text{ }^{\circ}\text{C/y}$. For warm permafrost ($-1.0\text{ to }-0^{\circ}\text{C}$) the average warming rate is $0.015\text{ }^{\circ}\text{C/y}$, and for permafrost with a temperature greater than -0.5°C it is only $0.011\text{ }^{\circ}\text{C/y}$. There is a stronger relationship between the warming rates and the AATD (Figure 8b including the QTP11). Permafrost with greater AATDs is warming rapidly while the warming rate is lower for permafrost with lower AATDs. For permafrost with average AATD below $0.5 \times 10^{-6}\text{ m}^2/\text{s}$ the warming rate is $0.017\text{ }^{\circ}\text{C/y}$, while for permafrost with average AATD greater than $0.5 \times 10^{-6}\text{ m}^2/\text{s}$ the warming rate is $0.020\text{ }^{\circ}\text{C/y}$. This phenomenon illustrates that the warming rates of permafrost are also controlled by the heat transfer capability and latent heat effects of the soil. The linkage between the warming rates and permafrost temperatures is not very strong because the warming rates are significantly affected by the regional climate change signal and local environmental factors such as vegetation and soil water content. However, AATD is a comprehensive indicator that reflects geothermal and regional environmental impacts at specific sites. Hence the relationships between the warming rate and the AATD is stronger than that between warming rate and permafrost temperature.

Based on the above discussion, we draw the conclusion that the thermal regime of permafrost has important implications for the distribution patterns of the thermal diffusivity of permafrost. The temperature-dependent adjustment of the thermal diffusivity has important implications for the rate of change of permafrost temperatures. In warm permafrost, the heat diffusion in the ground is slow and limited by the processes of latent heat exchange and the direct, measureable effects of climatic changes are considerably attenuated. The smaller AATD prevents heat transfer and more energy is partitioned into the thawing of the shallow permafrost, which will limit the immediate increase of permafrost temperature. In cold permafrost, the larger AATD will

enable ground temperature change at the same pace as that of the air temperature. The temperature of cold permafrost will increase more rapidly than that of warm permafrost under the same climatic warming. Thus we can predict the temporal evolution of permafrost by the estimate of the AATD using measurement data.

5 CONCLUSION

The thermal regime of warm permafrost has important implications on the rate of change of permafrost in the QTP. In warm permafrost regions, the latent heat effects buffered the heat exchange and the AATD is usually small, which buffered the heat transferred into the deep permafrost and results in small warming rates of permafrost. In cold permafrost, the AATD is greater because the latent heat effects are weak and result in a faster warming trend. At the same sites, thermal diffusivity is usually small at the active layer bottom since ice-water

REFERENCES

- Cheng, G. D., and Wu, T., H., 2007: Responses of permafrost to climate change and their environmental significance, Qinghai-Tibet Plateau. *Journal of Geophysical Research*, 112: F02S03. DOI: 10.1029/2006JF000631.
- Hinkel K.M. 1997. Estimating seasonal values of thermal diffusivity in thawed and frozen soils using temperature time series. *Cold Regions Science and Technology*, 26: 1-15
- Horton, R., Wierenga, P. J., and Nielsen, D. R. 1983. Evaluation of methods for determination apparent thermal diffusivity of soil near the surface, *Soil Sci. Soc. Am. J.*, 47: 23–32.
- Ingersoll, L. R., Zobel, O. J., Ingersoll, A. C., 1954: *Heat Conduction with Engineering, Geological and other applications*. McGraw-Hill, New York, p. 325.
- Jin, H. J., Sun, L. G., Wang, S. L., et al., 2008: Dual Influences of Local Environmental Variables on Ground Temperatures on the Interior-Eastern Qinghai-Tibet Plateau (I): Vegetation and Snow Cover. *Journal glaciology and geocryology* 30: 535-545.
- Qiu, G. Q., Liu, J. R., Liu, H. X., 1994: *Geocryological Glossary*. Lanzhou, Gansu Science Press: 28.
- Wang, L., Gao, Z., Horton, R. 2010. Comparison of Six Algorithms to Determine the Soil Apparent Thermal Diffusivity at a Site in the Loess Plateau of China. *Soil Science*, 175(2):51-60.
- Williams, P. J., Smith, M. W., 1989: *The frozen earth: Fundamentals of Geocryology*. Cambridge University Press, New York, USA.
- Wu, Q. B. and Zhang, T., 2008: Recent permafrost warming on the Qinghai-Tibetan Plateau. *Journal of Geophysical Research* 113, D13108, doi: 10.1029/2007JD009539.
- Wu, Q. B. and Zhang, T., 2010: Changes in active layer thickness over the Qinghai-Tibetan Plateau from 1995 to 2007, *Journal of Geophysical Research*, 115, D09107, doi:10.1029/2009JD012974.
- Xie, C.W., Zhao, L., Wu, T. H., Dong, X. C., 2012: Changes in the Thermal and Hydraulic Regime within the Active Layer in the Qinghai-Tibet Plateau. *Journal of Mountain Science*, 9: 483-491.
- Zhang, T., Osterkamp, T.E. 1995. Considerations in determining thermal diffusivity from temperature time series using finite difference methods. *Cold Regions Science and Technology* 23: 333-341.
- Zhao, L., Wu, Q. B., Marchenko, S. S., Sharkhuu, N., 2010: Thermal State of Permafrost and Active Layer in Central Asia during the international Polar Year. *Permafrost and Periglacial Process*, 21: 198-207.

Table 1 Geographical data and information on 17 monitoring sites on the QTP

Sites	Location		Areas	Altitude (m)	Established time	Daily data available
	Latitude	longitude				
QTB1	35° 42' 56" N	94° 04' 56" E	Xidatan	4230	1990.10	2006.01-2010.12
QTB2	35° 37' 32" N	94° 03' 34" E	Mt.Kunlun	4753	1990.10	2006.01-2010.12
QTB3	35° 31' 23" N	93° 47' 04" E	66Daoban	4560	1990.10	2006.01-2010.12
QTB4	35° 25' 50" N	93° 36' 01" E	Qinshuihe 203	4488	2005.10	2006.01-2010.12
QTB5	35° 21' 51" N	93° 26' 47" E	Chumaer River	4520	2005.10	2006.01-2010.12
QTB6	35° 17' 24" N	93° 16' 08" E	Hoh Xil Bridge	4563	2005.10	2006.01-2010.12
QTB7	35° 11' 36" N	93° 04' 26" E	Wudaoliang	4656	1990.10	2006.01-2010.12
QTB9	35° 08' 19" N	93° 02' 28" E	Hoh Xil	4804	2007.10	2006.01-2010.10
KKXL	35° 07' 59" N	93° 01' 59" E	Hoh Xil	4740	2005.10	2006.01-2010.12
BLH	34° 49' 46" N	92° 55' 57" E	Beilu River	4621	2002.10	2008.12-2010.10
WULI	34° 28' 39" N	92° 43' 33" E	Wuli	4571	2007.06	2008.12-2010.10
QTB11	34° 23' 13" N	92° 39' 22" E	Wuli	4623	2005.10	2006.01-2010.12
KXL	33° 57' 21" N	92° 20' 18" E	Kaixinlin	4726	2002.10	2006.01-2010.10
TTHN	33° 46' 23" N	92° 14' 05" E	Tongtian River	4886	2005.10	2006.01-2010.10
QTB15	33° 05' 51" N	91° 53' 52" E	Wenquan	4960	2005.10	2006.01-2010.12
QTB16	33° 04' 19" N	91° 56' 19" E	Tanggula	5100	2006.10	2006.07-2010.12
QTB18	31° 49' 07" N	91° 44' 12" E	Liangdaohe	4808	1975.10	2006.01-2010.12

Table 2. Climatic and environmental parameters at 18 monitoring sites on the QTP*

Sites	Climate Conditions		Permafrost Condition				Site descriptions
	MAAT (°C)	Precipitation (mm)	ALT (m)	DZA A (m)	MAGT (°C)	PT (m)	
QTB1	-2.0 to -4.5	300-350	1.65	6.4	-0.45	21.0	Sandy clay, flat surface, alpine grasslands
QTB2	-5.5 to -6.5	250-300	1.50	7.4	-2.25	-	Sandy clay, gentle slope, alpine grasslands
QTB3	-3.5 to -5.5	250-300	3.31	3.8	-0.41	-	Desertification surface, alpine grasslands
QTB4	-3.0 to -4.5	250-300	1.82	3.3	-0.35	20.0	Sandy clay, flat surface, alpine meadow
QTB5	-3.0 to -4.5	250-300	8.30	7.7	-0.03	5.2	Dissertation surface, alpine grasslands
QTB6	-3.0 to -4.5	250-300	3.32	3.9	-0.47	32.0	Sandy clay, flat surface, alpine grasslands
QTB7	-3.5 to -4.5	250-300	1.55	6.8	-1.53	-	Sandy clay, flat surface, alpine meadow
QTB9	-3.5 to -5.0	300-350	1.35	10.2	-2.70	-	Silt, Clay, flat surface, alpine meadow
KKXL	-3.5 to -5.0	300-350	1.58	10.3	-2.54	-	Sandy clay, flat surface, alpine meadow
BLH	-2.5 to -4.5	250-350	2.10	6.8	-0.34	21.5	Silt, Clay, flat surface, alpine meadow
WULI	-2.8 to -4.0	250-350	3.32	6.3	-0.45	24.0	Sandy clay, flat surface, alpine grasslands
QTB11	-2.8 to -4.0	250-350	2.71	14.9	1.90	-	Dissertation surface, alpine grasslands
KXL	-3.0 to -5.0	250-350	2.74	6.5	-0.55	-	Sandy clay, gentle slope, alpine grasslands
TTHN	-3.0 to -5.0	250-350	2.80	6.5	-0.48	26.5	Sandy clay, flat surface, alpine meadow
QTB15	-3.5 to -5.0	250-350	2.35	14.5	-1.03	-	Gravel and sandy, alpine grasslands
QTB16	-4.0 to -5.5	300-350	3.15	17.4	-1.25	-	Gravel, silt, gentle slope, alpine grasslands
QTB18	-1.8 to -2.5	350-450	1.25	8.2	-0.73	-	clay, flat surface, alpine meadow

MAAT: mean annual air temperature; ALT: active layer thickness; DZAA: the depths of zero annual amplitude; MAGT: mean annual ground temperature at the DZAA; PT: permafrost thickness.